

Update on the worsening particle radiation environment observed by CRaTER and implications for future human deep-space exploration

N. A. Schwadron^{1,2}, F. Rahmanifard¹, J. Wilson^{1,2}, A. P. Jordan^{1,2}, H. E. Spence^{1,2}, C. J. Joyce¹, J. B. Blake³, A. W. Case⁴, W. de Wet⁵, W. M. Farrell^{6,2}, J. C. Kasper⁷, M. D. Looper³, N. Lugaz¹, L. Mays⁶, J. E. Mazur³, J. Niehof¹, N. Petro⁶, C. W. Smith¹, L. W. Townsend⁵, R. Winslow¹, and C. Zeitlin⁸

Corresponding author: N. A. Schwadron, Institute for the Study of Earth, Oceans and Space, Space Science Center, Department of Physics, University of New Hampshire, 8 College Road, Durham NH, 03824 (nschwadron@unh.edu)

¹University of New Hampshire, Space Science Center, Durham, NH 03824, USA

²Solar System Exploration Research Virtual Institute, NASA Ames Research Center, Moffett Field, CA 94035-0001, USA

³The Aerospace Corporation, El Segundo, CA 90245-4609, USA

This article has been accepted for publication and undergone full peer review but has not been through the copyediting, typesetting, pagination and proofreading process, which may lead to differences between this version and the Version of Record. Please cite this article as doi: 10.1002/2017SW001803

Abstract. Over the last decade, the solar wind has exhibited low densities and magnetic field strengths, representing anomalous states that have never been observed during the space age. As discussed by Schwadron et al. (2014a), the cycle 23–24 solar activity led to the longest solar minimum in more than 80 years and continued into the “mini” solar maximum of cycle 24. During this weak activity, we observed galactic cosmic ray fluxes that exceeded the levels observed throughout the space age, and we observed small solar energetic particle events. Here, we provide an update to the Schwadron et al (2014a) observations from the Cosmic Ray Telescope for the Effects of

⁴High Energy Astrophysics Division,
Harvard Smithsonian Center for
Astrophysics, Cambridge, MA 02138, USA

⁵Dept of Nuclear Engineering, University
of Tennessee, Knoxville, TN, 37996

⁶Goddard Space Flight Center, Greenbelt,
MD 20771, USA

⁷Department of Climate and Space
Science, University of Michigan, Ann Arbor,
MI 48109-2143, USA

⁸Leidos Innovations Corporation,
Houston, TX 77042, USA

Radiation (CRaTER) on the Lunar Reconnaissance Orbiter (LRO). The Schwadron et al. (2014a) study examined the evolution of the interplanetary magnetic field, and utilized a previously published study by Goelzer et al. (2013) projecting out the interplanetary magnetic field strength based on the evolution of sunspots as a proxy for the rate that the Sun releases coronal mass ejections (CMEs). This led to a projection of dose rates from galactic cosmic rays on the lunar surface, which suggested a $\sim 20\%$ increase of dose rates from one solar minimum to the next, and indicated that the radiation environment in space may be a worsening factor important for consideration in future planning of human space exploration. We compare the predictions of Schwadron et al. (2014a) with the actual dose rates observed by CRaTER in the last 4 years. The observed dose rates *exceed* the predictions by $\sim 10\%$, showing that the radiation environment is worsening more rapidly than previously estimated. Much of this increase is attributable to relatively low-energy ions, which can be effectively shielded. Despite the continued paucity of solar activity, one of the hardest solar events in almost a decade occurred in Sept 2017 after more than a year of all-clear periods. These particle radiation conditions present important issues that must be carefully studied and accounted for in the planning and design of future missions (to the Moon, Mars, asteroids and beyond).

1. Introduction

Galactic Cosmic Rays (GCR) and Solar Energetic Particles (SEPs) pose significant challenges to long-duration crewed missions to deep space. The human biological consequences of particle radiation range from acute effects (radiation sickness) to long-term effects [c.f., *NRC*, 2008] including cancer induction, organ damage (including the heart, brain, and central nervous system). Risk associated with radiation hazards are typically quantified as a function of the effective dose that is related to the energy per unit mass (expressed in Gy=joule/kg) absorbed by biological tissue, and weighted according to the effectiveness of radiation damage in biological tissue. In this paper, we use recent measurements from the CRaTER instrument [Cosmic Ray Telescope for the Effects of Radiation, *Spence et al.*, 2010] on the Lunar Reconnaissance Orbiter (LRO) to determine dose rates (data available at <http://prediccs.sr.unh.edu/craterweb>) .

The deep solar cycle 23–24 minimum and the activity that followed in cycle 24 differed significantly from those of the prior solar cycles during the space age [*Schwadron et al.*, 2011; *McComas et al.*, 2013; *Schwadron et al.*, 2014b]. Most recently, *Rahmanifard et al.* [2017] concluded that we may be entering an era of extremely low solar activity, such as a Dalton minimum, a Gleissberg minimum or a Maunder minimum. Specifically, *Rahmanifard et al.* [2017] studied the recent trends in the evolution of the heliospheric magnetic field (HMF) in the context of past solar grand minima, especially the Maunder period (1645–1715) to gain further insight. A time series of the HMF was reconstructed from geomagnetic data and measurements from near-Earth spacecraft (OMNI) to find the timescales that control heliospheric field evolution through conversion from coronal mass

ejections (CMEs) into the ambient field, removal of the ambient field through magnetic reconnection, and interchange reconnection between CME and ambient magnetic flux. The minimum value for the HMF at 1 au in the reconstructed magnetic field is 3.13 ± 0.35 nT [Rahmanifard *et al.*, 2017], which is ~ 1 nT lower than observed in the deep cycle 23-24 minimum. Therefore, the analysis of Rahmanifard *et al.* [2017] suggests that while we have already observed significant weakening in solar activity, there exists the potential for far weaker activity in coming cycles.

Schwadron *et al.* [2014a] examined the radiation environment utilizing data from CRaTER and from PREDICCS [Predictions of Radiation from RElease, EMM-REM, and Data Incorporating the CRaTER, COSTEP, and other SEP measurements, <http://prediccs.sr.unh.edu> Schwadron, 2012]. PREDICCS provides for nowcasting the radiation environment near Earth, at the Moon, and near Mars. Figure 1 shows a key result of Schwadron *et al.* [2014a] indicating that dose rates (projected to the lunar surface) have grown in the last solar minimum to the highest level observed in the space age. A second major conclusion in Schwadron *et al.* [2014a] is that solar energetic particle (SEP) events have been quite weak during solar cycle 24. The probability of an SEP event exceeding either the 30-day or 1-year BFO limits is vanishingly small for deep space mission with at least 10 g/cm^2 shielding up to 1 year.

Schwadron *et al.* [2014a] were able to make a prediction for the evolution of the radiation environment on the lunar surface slightly beyond 2020. The basis of this prediction were the results of Goelzer *et al.* [2013], in which projections for the interplanetary magnetic field strength were made based on similarity of the solar cycle progression to the Dalton and Gleissberg minima. As seen in Figure 1, both projections showed that galactic cosmic

ray dose rates in the coming solar minimum between cycle 24 and 25 will be significantly higher ($\sim 20\%$) than the previous solar minimum. This results in a $\sim 20\%$ reduction in the time to reach a given level of risk of exposure-induced death (REID) for astronauts in interplanetary space. These findings show the pressing need to improve upon the understanding of the space radiation risk, predict likely clinical outcomes of interplanetary radiation exposure, and develop appropriate and effective mitigation strategies for future missions.

The purpose of this paper is to revisit the predictions of *Schwadron et al.* [2014a] with the benefit of 3.5 years of additional CRaTER data. In the discussion of weakening solar activity, we provide data on one of the largest SEP events of solar cycle 24 during September, 2017. Our paper is therefore included in the *Space Weather* special section, “Space Weather Events of 4–10 September 2017”. The paper is organized as follows: §2 describes the Cosmic Ray Telescope for the effects of Radiation; §3 describes the radiation environment due to evolving galactic cosmic fluxes; §4 describes the dose rates and accumulated doses observed during the September, 2017 SEP event; §5 describes interplanetary conditions near 1 au and modeling showing the configuration of successive coronal mass ejections (CMEs) giving rise to the September, 2017 SEP event; §6 provides conclusions.

2. Cosmic Ray Telescope for the Effects of Radiation

The CRaTER instrument consists of a linear stack of 3 pairs of thin and thick silicon detectors, labeled D1 through D6 (Spence et al., 2010, Figure 2). With CRaTER in its typical orientation, D1–D2 face deep space and the thin-thick detector pair D5–D6 faces the Moon. In this orientation, energetic particles originating from the zenith pass

through: 1) 0.81 mm (0.22 g/cm²) Al endcap, 2) D1—D2 detectors, 3) tissue-equivalent plastic (TEP) of thickness 54 mm (6.09 g/cm²), 4) D3—D4 detectors, 5) 27 mm (3.04 g/cm²) TEP, 6) D5—D6 detectors, and 7) 0.81 mm (0.22 g/cm²) Al endcap. Further details on CRaTER can be found in Spence et al. (2010). Significant energy loss occurs within the TEP. Therefore, D3—D4 are the most shielded detectors within the instrument.

The energy loss within the TEP allows us to differentiate between particles coming from the Moon and GCRs from deep space at energies below a few hundred MeV/nuc. As a particle traverses the detector stack, it loses energy, primarily within the TEP. Lower-energy particles deposit more energy in a detector than higher-energy particles. As a result, a coincident event that is registered in both D4 and D6 (both thick detectors) typically deposits a greater amount of energy in D4 than in D6 if it originates from the direction of the Moon. Conversely, if the particle originates from deep space, it will deposit a greater amount of energy in D6 than in D4, although at high energies, signals in the two detectors are indistinguishable. Note that the coincident rates in D4 and D6 from GCRs are larger than the coincident rates in D2 and D4 due to the larger field-of-view and the comparatively small energy loss within the TEP between D4 and D6 (the piece of TEP between D2 and D4 is thicker than the piece between D4 and D6).

The microdosimeter housed within CRaTER is an early version of what is now a commercially available hybrid that accurately measures total ionizing radiation dose in a silicon target (<http://www.teledynemicro.com/product/radiationdosimeter>). The CRaTER microdosimeter is behind about ~ 4.4 g/cm² equivalent aluminum, which shields against protons below ~ 55 MeV. *Mazur et al.* [2011] discussed the first six months of mission data

from the microdosimeter, and *Mazur et al.* [2015] updated the microdosimeter data from the start of the LRO mission through the end of 2014.

As in *Schwadron et al.* [2012] we correct the observed dose rate for the changing solid angle blocked by the Moon, and for the difference in energy deposition in water/tissue versus silicon. All dose rates and accumulated doses are adjusted to the lunar surface, where half of the sky is blocked by the Moon. When averaged over 12 h, the variations among the various orbit modes have less than a 5% and 20% effect on the galactic cosmic ray dose rate and peak solar proton dose rate, respectively.

3. Does the Galactic Radiation Hazard Continue to Worsen?

We test the predictions from *Schwadron et al.* [2014a] with new CRaTER data from 2014 through 2017 (Fig. 3, bright green). As detailed by *Schwadron et al.* [2014a], the measurements of ACE in Fig. 3 (red) result from fitting heavy ion distributions measured by ACE/CRIS [*Stone et al.*, 1998] to a model [*O'Neill*, 2006] for GCR distributions, which are then fed in to HZETRN 2005 to estimate associated dose rate. The data from ACE are provided up to 2010, after which we use dose rates measured by CRaTER (dark green points show CRaTER published previously, light green points show more recent data).

Model results are shown in Figure 3 (black curves prior to 2014, and blue and red curves after 2014) [*Schwadron et al.*, 2014a]. Sunspot numbers are used as a proxy for CME frequency (number of CMEs ejected per unit time). The ejection of successive CMEs introduces new magnetic flux into the heliosphere, thereby increasing the magnitude of the HMF. The low solar activity of the minimum between cycle 23 and 24 enabled steady disconnection of magnetic flux unbalanced by the addition of new magnetic flux from CMEs [*Connick et al.*, 2009]. The low heliospheric magnetic flux reduces the modulation

of GCRs and increases GCR fluxes. The dose rates shown in Figure 1 are therefore higher during the 2008–2009 activity lull compared to the 1997 solar minimum, and the mini-maximum in cycle 24 continues to show relatively weak solar activity.

Goelzer et al. [2013] showed that recent trends are consistent with the beginning of the 1790–1830 period (the Dalton minimum), or the beginning of the 1890–1920 period (the Gleissberg minimum) [*Smith et al.*, 2014]. Solar activity over the next ~ 5 years (through 2020) was estimated [*Goelzer et al.*, 2013; *Smith et al.*, 2014] based on the historic behavior in sunspot evolution for the Dalton-like minimum and the Gleissberg-like minimum. Recent CRaTER data (bright green points) obtained after the *Schwadron et al.* [2014a] study are compared to predictions in Figure 3. The CRaTER observations are enhanced relative to the predictions by $\sim 10\%$, demonstrating an even more rapid increase in radiation dose rates than associated with a Dalton-like or a Gleissberg-like minimum.

Cosmic-ray drifts are known to influence the time-evolution of galactic cosmic ray fluxes [*Jokipii et al.*, 1977]. The cosmic ray drift patterns depend on the quantity qA , where q is the cosmic ray charge and the sign of A corresponds to the dominant polarity of the northern heliospheric magnetic field. In cycles with $qA > 0$, cosmic rays drift inward near the poles and outward near the heliospheric current sheet. In these cycles, we typically observe “flat-topped” maxima in the time evolution of GCR fluxes. In contrast, cycles with $qA < 0$ have cosmic ray drift patterns outward near the poles, and inward near the current sheet causing “peaked” maxima in the time evolution of GCR fluxes [*Webber and Lockwood*, 1988; *Smith*, 1990]. For protons and cosmic rays with $q > 0$, which contribute most of the GCR dose, the solar minimum between cycles 23 and 24 had $qA < 0$ and a

peaked maximum in GCR flux, whereas the solar minimum between cycle 24 and 25 will have $qA > 0$ and a flat-topped maximum. The more rapid increase in dose rate reported here could be influenced by the change in cosmic ray drift patterns in the transition to the cycle 24-25 solar minimum. For this reason, it will be important to compare the shape of the maximum in dose rates observed by CRaTER in the timeframe of 2020 (the cycle 24-25 GCR flux maximum) with the peaked maximum previously observed in 2009 (the cycle 23-24 GCR flux maximum).

While these observations suggest the evolution toward a grand minimum, it is important to bear in mind that various solar activity models yield disparate predictions, due to a lack of understanding of the underlying mechanisms that drive solar activity. For example, in contrast to the prediction of a prolonged deep minimum, a model based on observations of the solar polar magnetic fields near solar minimum *Svalgaard* [2017] predicts that the cycle 25 maximum will be stronger than the cycle 24 maximum; this model accurately predicted the weak cycle 24 maximum *Svalgaard et al.* [2005]. Another well-known model *Hathaway and Upton* [2016] predicts that the cycle 25 maximum will be about the same as that of cycle 24. Neither of these scenarios is consistent with the onset of a grand minimum.

We also show an update for the sunspot numbers (black curve) in Figure 3 based on the international sunspot number released by Sunspot Index and Long-term Solar Observations (SILSO, <http://sidc.oma.be/silso/home>). In our 2014 paper we used the original international sunspot number, which has been updated since then to remove the conventional Zurich factor (0.6) and eliminate the effect of a new counting method applied in Zurich by reducing all numbers after 1947 by 18%

(<http://sidc.oma.be/press/01/welcome.html>). Since in our work we use sunspot number (SSN) as a proxy for the solar activity, we are primarily focused on the variations in SSN. In order to be consistent with our previous paper we adapt the new sunspot number data set from SILSO for equivalent sunspot numbers.

Recently, *Rahmanifard et al.* [2017] investigated the rate of CMEs from LASCO and performed a χ -square analysis to derive the relationship between sunspot number and CME rate. This analysis resulted in lower CME rate than used by *Goelzer et al.* [2013], and therefore an update to the modulation model developed by *Schwadron et al.* [2014a].

The minimum dose rate in Figure 3 near the end of 2014 is similar to the minimum dose rate observed, which is $\sim 40\%$ higher in cycle 24 as compared to cycle 23. This is important both because of the large increase in dose rate and because the inflection in dose rate is now observed by CRaTER with the addition of new data. The fact that the observed dose rates exceed the model prediction demonstrates that the paucity of solar activity continues to cause elevated cosmic ray fluxes and higher dose rates at this phase of the solar cycle than observed previously in the space age.

Modulation of GCRs by the interplanetary magnetic field is a stochastic process, and the relationship between a given level of activity and the resulting flux in the inner heliosphere is non-trivial. However, broadly speaking, modulation shifts the energy of ions in the local interstellar spectrum (LIS) to lower energies, and depletes the low-energy portion of the spectrum. During periods of weak modulation, fluxes of relatively low-energy ions (with kinetic energies below about 1 GeV/nuc) are enhanced compared to periods of strong modulation, but a significant share of these ions have ranges that are insufficient to penetrate moderate depths of shielding. This is particularly true for high-charge ions

due to the Z^2 dependence of ionization energy loss, and these ions contribute significantly to dose in free space or under thin shielding. Less dramatic increases in dose rates are seen when shielding is more substantial. For example, the NASA OLTARIS model *Singleterry et al.* [2011] predicts that 30 g cm^{-2} of aluminum shielding produces a roughly 10% decrease in dose rate for solar minimum conditions, and a roughly 15% increase under solar maximum conditions, tending to blunt the changes in the incident GCR fluxes.

4. The Solar Energetic Particle Hazard During Periods of Weak Activity

Schwadron et al. [2014a] studied the probability of SEP events using PREDICCS [Schwadron, 2012]. They found that the probability of reaching the 30-day Blood Forming Organ (BFO) dose limit of 25 cGy-equivalent behind 10 g/cm^2 aluminum shielding was insignificant over time-scales of 30 days 1 year [NRC, 2008].

While the cycle 24 conditions indicate a low probability for an extreme event, the recent September 10 2017 SEP event demonstrates that large events can arise with little warning. Figure 4 shows the dose rates in the D1–D2, D3–D4, D5–D6 detectors and CRaTER microdosimeter; the > 1.5 year lull in activity in 2016–2017 is obvious. The recent September 2017 event was one of the largest of the CRaTER mission, and was rivaled only the March 13 2012 SEP event in terms of the most shielded D3–D4 and microdosimeter dose rates.

The September 2017 event had an unusually hard spectrum, with large fluxes above 400 MeV, and large dose rates in the most shielded CRaTER detectors. Figure 5 shows the accumulated dose during the event as a function of location and shielding in the CRaTER detector stack accumulated during the event along with the PREDICCS doses modeled through the event into $1 \text{ g/cm}^2 \text{ H}_2\text{O}$, a proxy for a Lens or skin dose.

In Figure 5, we combined CRaTER observations (yellow triangles) with data from PREDICCS (red points). The blue line and shaded uncertainty region represents a power-law fit to the PREDICCS data. The functional form of accumulated dose vs. shielding plotted in Figure 5 allows us to estimate the effective shielding (in g/cm^2) for each of the CRaTER detector pairs. The shielding estimates are roughly consistent with the average shielding provided by the TEP, endcaps, and the side-shielding that encircles all six detectors. These effective shielding depths will be useful in estimating the effects of shielding and the attenuation of dose within materials of varying thickness.

These CRaTER shielding estimates for detector pairs are roughly consistent with the shielding associated with the TEP and endcaps. However, radiation penetrates CRaTER from all directions not blocked by the Moon. For example, the endcap provides $0.22 \text{ g}/\text{cm}^2$ Al shielding. However, we find effective D1–D2 shielding of $0.37 \pm 0.02 \text{ g}/\text{cm}^2$, which is in excess of the endcap shielding due to extra mass around the detector pair and increased shielding from side-penetrating radiation.

An important question is the degree to which the September, 2017 could have significant health effects for astronauts. We find from Figure 5 that the lens and skin dose on the lunar surface would approach the 30-day limits (100 cGy skin dose and 150 cGy lens dose) [Cucinotta *et al.*, 2010; NRC, 2008; NCRP, 2000]. However, even moderate shielding ($> 1 \text{ g}/\text{cm}^2$ Al shielding) would reduce the radiation dose below these limits. A question is whether the dose would approach radiation limits during an extravehicular activity (EVA), typically lasting ~ 3 hrs. At the peak skin/lens dose rate of $5.8 \pm 0.3 \text{ cGy}/\text{hr}$ behind $0.3 \text{ g}/\text{cm}^2$ Al shielding, an astronaut would collect $17.4 \pm 0.9 \text{ cGy}$ dose within 3 hrs, which is significantly lower than lens/skin dose limits. This dose and dose rate

would be approximately doubled in free-space, also below the 30-day limits. Both the accumulated doses during the September 2017 event, and the maximum dose rate are significantly smaller than those in extreme SEP events, such as the August 1972 event. For example, the skin dose and maximum skin dose rate behind thin shielding (Al 0.3 g/cm²) during the August 1972 event was 3215 cGy and 980.90 cGy/hr [Hu et al., 2009], more than a decade larger than observed in the September, 2017 event.

The precise biological effects of SEP radiation remains an area of active research [e.g., Cucinotta and Durante, 2006; Cucinotta et al., 2010; Schwadron et al., 2014a]. It is clear that the September 2017 event is dangerous, with doses that are large, but not conspicuously above limits defined by the radiation biology community. An event of this kind represents an example in which astronauts would ideally be located behind the safety of spacecraft shielding. As such, advance warning for such events remains an imperative.

We conclude this section by noting that the accumulated dose in the September 2017 SEP event approached 30-day limits for low shielding thickness. The analysis demonstrates that the hard spectrum substantiated a radiation hazard. The fact that the event arose during a period of relatively quiet solar activity, while not uncommon for the declining phase, suggests that these events may be difficult to predict. However, as discussed in the next section, the event shows an evolution generally consistent with twin-CME scenarios studied by Li et al. [2012] and Lugaz et al. [2017].

5. Successive CMEs in Development of the September 2017 SEP events

The detailed evolution of the SEP events in Sept 2017 are shown in Figure 6. These include two X-class flares that started each of the major events on September 6 and September 10. Note that the multiple eruptions of the same active region at the Sun

created a energetic particle seed population that was subsequently accelerated in the September 10 event, similar to twin-CME scenarios studied by *Li et al.* [2012] and *Lugaz et al.* [2017].

Both of the X-class flares in September were associated with large and fast interplanetary coronal mass ejections (ICMEs). Figure 7 shows the Wang-Sheeley-Argge (WSA)-ENLIL model [*Odstrcil et al.*, 2005] with cone extension for simulating propagation of ICMEs. The simulations were run at the Community Coordinated Modeling Center (CCMC), with the run *Leila_Mays_101017_SH.5* and model version number ENLIL 2.8. The model input parameters for the ICME are as follows: latitude=-15 degrees, longitude=24 degrees, half-width=50 degrees, speed=1850 km/s, and a CME leading edge time of 2017-09-06 14:00 UT at the ENLIL inner boundary of 21.5 Rs. For the second ICME the model input parameters are: latitude=-10 degrees, longitude=92 degrees, half-width=70 degrees, speed=2800 km/s, and a CME leading edge time of 2017-09-10 17:12 UT at the ENLIL inner boundary of 21.5 Rs. Left panels in Figure 7 show simulated density in the ecliptic plane from 9/6/2017 through 9/8/2017 during the first of the major ICME events. The density enhancement in front of the black contour represents the piled up ICME sheath material. Right panels in Figure 7 show simulated plasma speed in the ecliptic plane. In this case we observe a fast ICME driving a strong compression that presumably forms a shock that sweeps over Earth near 9/8/2017. Note that the modeled fast wind driving the shock that sweeps over Earth has a speed exceeding 900 km/s.

Figure 8 shows the 1 au plasma signatures observed by ACE at 1 au during the passage of the ICME released after the September 6 X9.3 flare. We show (pink vertical lines) the ICME start time, the ICME Magnetic Ejecta (ME) start time, and the ICME end

time. The magnetic field and plasma velocity both show the passage of a shock near the beginning of 9/8/2017. The maximum plasma speed is observed slightly in excess of 800 km/s. At the ME start time t_0 , there is a decrease in magnetic variability, and a clear rotation in the magnetic field. Around the same place where ME starts there is also a decrease in temperature, and the steady decrease in plasma speed. This ICME was directed at Earth, so we observe the ME.

Trailing behind the ICME is a rarefaction region where the density becomes low ($> 0.23 \text{ cm}^{-3}$) while the magnetic field strength remains close to nominal. As a result, the Alfvén speed becomes large and the Alfvénic Mach number becomes relatively low, > 1.3 . Even lower densities and Alfvénic Mach numbers may be obscured by several data gaps: ACE data gap from 09/09 01:30 to 09/11 00:00 and Wind data gap from 09/10 03:00 to 09/11 00:00. These conditions are reminiscent of density anomaly observed in May, 1999 [Usmanov *et al.*, 2000]. Analysis of this rarefaction region is ongoing.

The WSA-ENLIL simulation of the ICME released after the September 10 flare is shown in Figure 9. The WSA-ENLIL model runs from September 10, 2017 through September 12, 2017 show the propagation of the CME from the Sun to 1 au. This second large ICME was directed much closer to the STEREO-B direction, at longitudes more than 90° larger than that of Earth. Only a small portion of the modeled sheath of the ICME sweeps past Earth.

The ICME sheath appears well connected to Earth throughout the propagation of the CME from the Sun to 1 au. This indicates that the energetic particles accelerated from the CME sheath can propagate to Earth throughout the period in which the ICME propagates to 1 au. The *in situ* plasma signatures observed at 1 au (Figure 10) also show

evidence of the compressed ICME sheath, and magnetic ejecta; however both structures are significantly smaller and weaker than in the ICME observed on September 8.

A key question is how large events such as the September 10, 2017 event arise. The answer must take into account many factors including: (1) the size, speed and shock or compression characteristics of the CME and ICME driver; (2) the magnetic connectivity throughout the event [e.g., *Schwadron et al.*, 2015] and (3) the existence of suprathermal seed populations [e.g., *Schwadron et al.*, 1996; *Desai et al.*, 2003, 2006].

The case observed appears to have all the ingredients necessary for extremely high-energy particle acceleration: (1) the CMEs released on September 6 and September 10 were large and fast (speeds > 600 km/s); (2) there was direct magnetic connectivity between the CME shock or compression and Earth throughout the propagation of both events; (3) the first of the CME events created a large energetic particle seed population accelerated further during the passage of the second CME [consistent with the twin-CME scenario *Li et al.*, 2012] ; and (4) we are well-connected to the flank of the second ICME, where the shock is quasi-perpendicular, which is likely more efficient for particle acceleration [e.g., *Schwadron et al.*, 2015],

Figure 11 summarizes the successive CME events causing particle acceleration to high energies. The first September 6 event showed the clear signature of enhanced energetic storm particles (ESP) accelerated by the shock during the passage of the Earth-directed ICME. In contrast, the second ICME showed only a small ESP enhancement near 9/12 20:00 UT during passage of the ICME shock. In fact, the peak fluxes occurred when the CME was relatively close to the Sun.

The observed acceleration by successive ICMEs is well-known to be a powerful energetic particle accelerator [*Gopalswamy et al.*, 2004; *Li et al.*, 2012; *Lugaz et al.*, 2017]. The first CME causes enhancements in energetic particles throughout the inner heliosphere. In fact, prior to the beginning of the September 10 event, we observe energetic particle enhancements up to at least 30 MeV. Further, throughout the event we continue to see the more rapid decay of energetic particles above 30 MeV after the passage of the ICME shock near the beginning of September 8, 2017, suggesting that energetic particles continue to diffuse out from the region inside of 1 au. During the acceleration of the second CME, an energetic particle population already exists, which then significantly increases the seed population fed into acceleration. This appears to be a scenario ideal for acceleration from the flanks of the second expanding and accelerating CME close to the Sun [*Schwadron et al.*, 2015].

6. Summary and Conclusions

We have shown that there has been a rapid GCR recovery in the approach to solar minimum over the period from 2014 to 2017. Previously *Schwadron et al.* [2014a] studied the evolution of GCR dose rate through solar cycles throughout the space age, concluding that the coming solar minimum will show increased fluxes and dose rates associated with GCRs compared to previous minima. GCR dose rates are increasing at a rate faster than predicted by *Schwadron et al.* [2014a].

Despite the low solar activity of cycle 24 and the continued weakening of solar activity in the descending phase, we have observed a relatively large SEP event in September of 2017. The event appeared as the result of successive fast CMEs, the first released on September 6, 2017 directed at Earth, and the second released on September 10, 2017 directed >

90° longitudinally forward with respect to Earth. Both events were magnetically well-connected, but the enhanced energetic particle populations accelerated in the first event were subsequently accelerated in the second CME event. These observations provide strong support for particle acceleration by successive ICMEs [*Gopalswamy et al.*, 2004; *Li et al.*, 2012; *Lugaz et al.*, 2017].

We conclude that we are likely in an era of decreasing solar activity. The activity is weaker than observed in the descending phases of previous cycles within the space age, and even weaker than the predictions by *Schwadron et al.* [2014a]. We continue to observe large but isolated SEP events, the latest one occurring in September of 2017 caused largely by particle acceleration from successive magnetically well-connected CMEs. The radiation environment remains a critical factor with significant hazards associated both with historically large galactic cosmic ray fluxes and large but isolated SEP events.

Acknowledgments. We thank all those who made CRaTER possible. CRaTER is primarily funded by the LRO program (Contract No. NNG11PA03C). This work was also funded EMMREM (grant number NNX07AC14G), C-SWEPA (NASA grant number NNX07AC14G), Sun-2-Ice (NSF grant number AGS1135432) projects, DoSEN (NASA grant NNX13AC89G), DREAM2 (NASA grant NNX14AG13A), NASA STTR Phase 1 and 2 (A Coupled System for Predicting SPE Fluxes, Contract NNX15CG52P). CRaTER data are available at <http://crater-web.sr.unh.edu>. PREDICCS data are available at <http://prediccs.sr.unh.edu>.

References

Connick, D. E., C. W. Smith, and N. A. Schwadron (2009), The Flux of Open and

Toroidal Interplanetary Magnetic Field as a Function of Heliolatitude and Solar Cycle, *Astrophys. J.*, 695, 357–362, doi:10.1088/0004-637X/695/1/357.

Cucinotta, F. A., and M. Durante (2006), Cancer risk from exposure to galactic cosmic rays: implications for space exploration by human beings, *J.-Lancet Oncology*, 7, 431.

Cucinotta, F. A., S. Hu, N. A. Schwadron, K. Kozarev, L. W. Townsend, and M.-H. Y. Kim (2010), Space radiation risk limits and Earth-Moon-Mars environmental models, *Space Weather*, 8, S00E09, doi:10.1029/2010SW000572.

Desai, M. I., G. M. Mason, J. R. Dwyer, J. E. Mazur, R. E. Gold, S. M. Krimigis, C. W. Smith, and R. M. Skoug (2003), Evidence for a Suprathermal Seed Population of Heavy Ions Accelerated by Interplanetary Shocks near 1 AU, *Astrophys. J.*, 588, 1149–1162, doi:10.1086/374310.

Desai, M. I., G. M. Mason, J. E. Mazur, and J. R. Dwyer (2006), Solar Cycle Variations in the Composition of the Suprathermal Heavy-Ion Population near 1 AU, *Astrophys. J. Lett.*, 645, L81–L84, doi:10.1086/505935.

Goelzer, M. L., C. W. Smith, N. A. Schwadron, and K. G. McCracken (2013), An analysis of heliospheric magnetic field flux based on sunspot number from 1749 to today and prediction for the coming solar minimum, *Journal of Geophysical Research (Space Physics)*, 118, 7525–7531, doi:10.1002/2013JA019404.

Gopalswamy, N., S. Yashiro, S. Krucker, G. Stenborg, and R. A. Howard (2004), Intensity variation of large solar energetic particle events associated with coronal mass ejections, *J. Geophys. Res.*, 109(A18), 12,105, doi:10.1029/2004JA010602.

Hathaway, D. H., and L. A. Upton (2016), Predicting the amplitude and hemispheric asymmetry of solar cycle 25 with surface flux transport, *Journal of Geophysical Research*

(*Space Physics*), 121(A10), 10, doi:10.1002/2016JA023190.

Hu, S., M.-H. Y. Kim, G. E. McClellan, and F. A. Cucinotta (2009), Modeling the acute health effects of astronauts from exposuite to large solar particle events, *Health Physics*, 96, 465 – 476, doi:10.1097/01.HP.0000339020.92837.61.

Jokipii, J. R., E. H. Levy, and W. B. Hubbard (1977), Effects of particle drift on cosmic-ray transport. i - general properties, application to solar modulation, *Astrophys. J.*, 213, 861–868, doi:10.1086/155218.

Li, G., R. Moore, R. A. Mewaldt, L. Zhao, and A. W. Labrador (2012), A Twin-CME Scenario for Ground Level Enhancement Events, *Space Sci. Rev.*, 171, 141–160, doi:10.1007/s11214-011-9823-7.

Lugaz, N., M. Temmer, Y. Wang, and C. J. Farrugia (2017), The Interaction of Successive Coronal Mass Ejections: A Review, *Solar Phys.*, 292, 64, doi:10.1007/s11207-017-1091-6.

Mazur, J. E., W. R. Crain, M. D. Looper, D. J. Mabry, J. B. Blake, A. W. Case, M. J. Golightly, J. C. Kasper, and H. E. Spence (2011), New measurements of total ionizing dose in the lunar environment, *Space Weather*, 9, S07002, doi:10.1029/2010SW000641.

Mazur, J. E., C. Zeitlin, N. Schwadron, M. D. Looper, L. W. Townsend, J. B. Blake, and H. Spence (2015), Update on Radiation Dose From Galactic and Solar Protons at the Moon Using the LRO/CRaTER Microdosimeter, *Space Weather*, 13, 363–364, doi:10.1002/2015SW001175.

McComas, D. J., N. Angold, H. A. Elliott, G. Livadiotis, N. A. Schwadron, R. M. Skoug, and C. W. Smith (2013), Weakest solar wind of the space age and the current "Mini" solar maximum, *The Astrophysical Journal*, 779, 2, doi:10.1088/0004-637X/779/1/2.

NCRP (2000), *Radiation protection guidance for activities in low-Earth orbit*, NCRP Report 132, National Council on Radiation Protection and Measurements, Bethesda (MD).

NRC (2008), *Managing Space Radiation Risk in the New Era of Space Exploration*, National Academy Press, The National Academies Press, Washington, DC.

Odstrcil, D., V. J. Pizzo, and C. N. Arge (2005), Propagation of the 12 May 1997 interplanetary coronal mass ejection in evolving solar wind structures, *Journal of Geophysical Research (Space Physics)*, *110*, A02106, doi:10.1029/2004JA010745.

O'Neill, P. M. (2006), Badhwar O'Neill galactic cosmic ray model update based on advanced composition explorer (ACE) energy spectra from 1997 to present, *Advances in Space Research*, *37*, 1727–1733, doi:10.1016/j.asr.2005.02.001.

Rahmanifard, F., N. A. Schwadron, C. W. Smith, K. G. McCracken, K. A. Duderstadt, N. Lugaz, and M. L. Goelzer (2017), Inferring the Heliospheric Magnetic Field Back through Maunder Minimum, *Astrophys. J.*, *837*, 165, doi:10.3847/1538-4357/aa6191.

Schwadron, N. (2012), Near-real-time situational awareness of space radiation hazards, *Space Weather*, *10*, 10,005, doi:10.1029/2012SW000860.

Schwadron, N. A., L. A. Fisk, and G. Gloeckler (1996), Statistical acceleration of interstellar pick-up ions in co-rotating interaction regions, *GRL*, *23*, 2871–2874, doi:10.1029/96GL02833.

Schwadron, N. A., C. W. Smith, H. E. Spence, J. C. Kasper, K. Korreck, M. L. Stevens, B. A. Maruca, K. K. Kiefer, S. T. Lepri, and D. McComas (2011), Coronal electron temperature from the solar wind scaling law throughout the space age, *The Astrophysical Journal*, *739*, 9, doi:10.1088/0004-637X/739/1/9.

Schwadron, N. A., T. Baker, B. Blake, A. W. Case, J. F. Cooper, M. Golightly, A. Jordan, C. Joyce, J. Kasper, K. Kozarev, J. Mislinski, J. Mazur, A. Posner, O. Rother, S. Smith, H. E. Spence, L. W. Townsend, J. Wilson, and C. Zeitlin (2012), Lunar radiation environment and space weathering from the cosmic ray telescope for the effects of radiation (CRaTER), *Journal of Geophysical Research (Planets)*, *117*, doi:10.1029/2011JE003978.

Schwadron, N. A., J. B. Blake, A. W. Case, C. J. Joyce, J. Kasper, J. Mazur, N. Petro, M. Quinn, J. A. Porter, C. W. Smith, S. Smith, H. E. Spence, L. W. Townsend, R. Turner, J. K. Wilson, and C. Zeitlin (2014a), Does the worsening galactic cosmic radiation environment observed by CRaTER preclude future manned deep space exploration?, *Space Weather*, *12*, 622–632, doi:10.1002/2014SW001084.

Schwadron, N. A., M. L. Goelzer, C. W. Smith, J. C. Kasper, K. Korreck, R. J. Leamon, S. T. Lepri, B. A. Maruca, D. McComas, and M. L. Steven (2014b), Coronal electron temperature in the protracted solar minimum, the cycle 24 mini maximum, and over centuries, *Journal of Geophysical Research: Space Physics*, doi:10.1002/2013JA019397.

Schwadron, N. A., M. A. Lee, M. Gorby, N. Lugaz, H. E. Spence, M. Desai, T. Török, C. Downs, J. Linker, R. Lionello, Z. Mikić, P. Riley, J. Giacalone, J. R. Jokipii, J. Kota, and K. Kozarev (2015), Particle Acceleration at Low Coronal Compression Regions and Shocks, *Astrophys. J.*, *810*, 97, doi:10.1088/0004-637X/810/2/97.

Singleterry, R. C., Jr., S. R. Blattng, M. S. Cloudsley, G. D. Qualls, C. A. Sandridge, L. C. Simonsen, T. C. Slaba, S. A. Walker, F. F. Badavi, J. L. Spangler, A. R. Aumann, E. N. Zapp, R. D. Rutledge, K. T. Lee, R. B. Norman, and J. W. Norbury (2011), OLTARIS: On-line tool for the assessment of radiation in space, *Acta Astronautica*, *68*,

1086–1097, doi:10.1016/j.actaastro.2010.09.022.

Smith, C. W., K. G. McCracken, N. A. Schwadron, and M. L. Goelzer (2014), The heliospheric magnetic flux, solar wind proton flux, and cosmic ray intensity during the coming solar minimum, *Space Weather*, *12*, 499–507, doi:10.1002/2014SW001067.

Smith, E. J. (1990), The heliospheric current sheet and modulation of Galactic cosmic rays, *J. Geophys. Res.*, *95*, 18,731–18,743, doi:10.1029/JA095iA11p18731.

Spence, H. E., A. W. Case, M. J. Golightly, T. Heine, B. A. Larsen, J. B. Blake, P. Caranza, W. R. Crain, J. George, M. Lalic, A. Lin, M. D. Looper, J. E. Mazur, D. Salvaggio, J. C. Kasper, T. J. Stubbs, M. Doucette, P. Ford, R. Foster, R. Goeke, D. Gordon, B. Klatt, J. O'Connor, M. Smith, T. Onsager, C. Zeitlin, L. W. Townsend, and Y. Charara (2010), CRaTER: the cosmic ray telescope for the effects of radiation experiment on the lunar reconnaissance orbiter mission, *Space Science Reviews*, *150*, 243–284, doi:10.1007/s11214-009-9584-8.

Stone, E. C., C. M. S. Cohen, W. R. Cook, A. C. Cummings, B. Gauld, B. Kecman, R. A. Leske, R. A. Mewaldt, M. R. Thayer, B. L. Dougherty, R. L. Grumm, B. D. Milliken, R. G. Radocinski, M. E. Wiedenbeck, E. R. Christian, S. Shuman, H. Trexel, T. T. von Rosenvinge, W. R. Binns, D. J. Crary, P. Dowkontt, J. Epstein, P. L. Hink, J. Klarmann, M. Lijowski, and M. A. Olevitch (1998), The cosmic-ray isotope spectrometer for the advanced composition explorer, *Space Science Reviews*, *86*, 285–356, doi:10.1023/A:1005075813033.

Svalgaard, L. (2017), Observations of polar magnetic fields and cycle 25 prediction, in *Solar Cycle 25 Prediction Workshop*, The, Nagoya University, Aichi, Japan.

Svalgaard, L., E. W. Cliver, and Y. Kamide (2005), Sunspot cycle 24: Smallest cycle in 100 years?, *Geophys. Res. Lett.*, *32*, L01104, doi:10.1029/2004GL021664.

Usmanov, A. V., M. L. Goldstein, and W. M. Farrell (2000), A view of the inner heliosphere during the May 10-11, 1999 low density anomaly, *Geophys. Res. Lett.*, *27*, 3765–3768, doi:10.1029/2000GL000082.

Webber, W. R., and J. A. Lockwood (1988), Characteristics of the 22-year modulation of cosmic rays as seen by neutron monitors, *J. Geophys. Res.*, *93*, 8735–8740, doi:10.1029/JA093iA08p08735.

Accepted Article

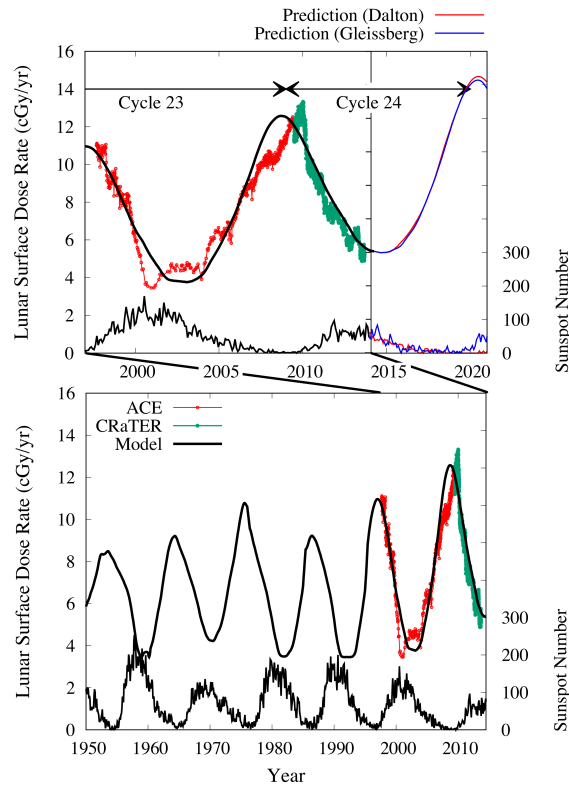


Figure 1. Evolving and increasingly hazardous radiation levels in space. Top Panel: ACE dose rates (red) are based on fits to CRIS spectra [O'Neill, 2006], CRaTER measurements (green) from the zenith facing D1/D2 detectors are used as proxies for lens dose rates behind 0.3 g/cm^2 Al shielding Schwadron *et al.* [2012]. The sunspot number predictions (the lower blue and red dashed lines) show two cases based on a Gleissberg-like and a Dalton-like minimum, the results of which are similar. The dose predictions (solid black curve and the upper blue and red curves) are from a sunspot-based model of the heliospheric magnetic field and the correlated variation in modulation of GCRs [Appendix A Schwadron *et al.*, 2014a]. The ACE data, CRaTER data, and model results are projected to the lunar surface. Bottom Panel: Same as top panel but for a longer time span. [From Schwadron *et al.*, 2014a].

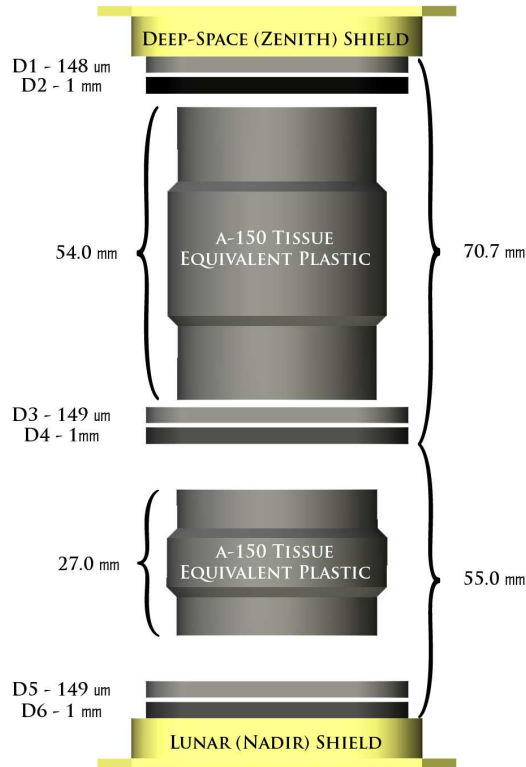


Figure 2. The CRaTER instrument consists of a stack of 3-pairs of thin and thick silicon detectors separated by tissue-equivalent plastic (TEP). Shown here is the configuration of these detectors with D1–D2 facing zenith, and D5–D6 facing in the nadir direction. Note that the D3–D4 detectors are the most shielded thin-thick pair within the instrument.

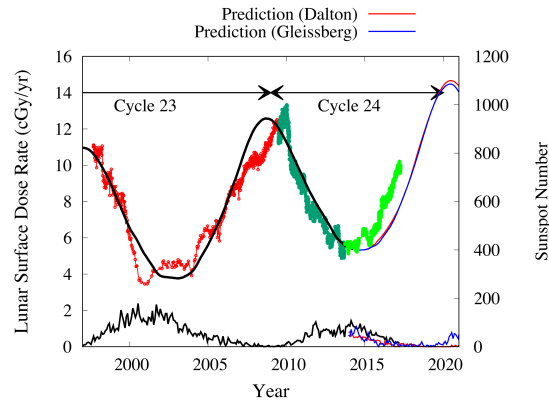


Figure 3. Recent CRaTER data (bright green) are updated after the *Schwadron et al.* [2014a] study to further test the predictions. The sunspot number *predictions* from *Goelzer et al.* [2013] (the lower blue and red curves) show two cases based on a Gleissberg-like and a Dalton-like minimum, the results of which are similar. Updates to the sunspot number (lower black curve) are adapted from the international sunspot number released by Sunspot Index and Long-term Solar Observations (SILSO, <http://sidc.oma.be/silso/home>). The dose predictions (solid black curve and the upper red and blue curves) are from a sunspot-based model of the heliospheric magnetic field and the correlated variation in modulation of GCRs [Appendix A *Schwadron et al.*, 2014a]. The ACE data, CRaTER data, and model results are projected geometrically to the lunar surface.

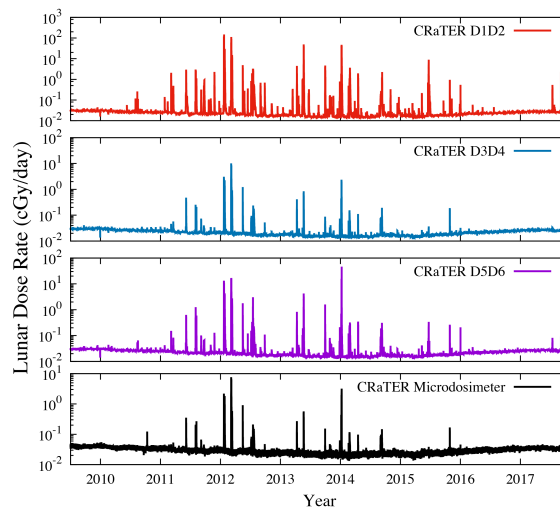


Figure 4. Dose rates in the three thin-thick detector pairs (D1–D2, D3–D4, D5–D6) and the microdosimeter within CRaTER. All dose rates have been geometrically corrected for exposure on the lunar surface and corrected for doses in H_2O as opposed to Si [Schwadron *et al.*, 2012].

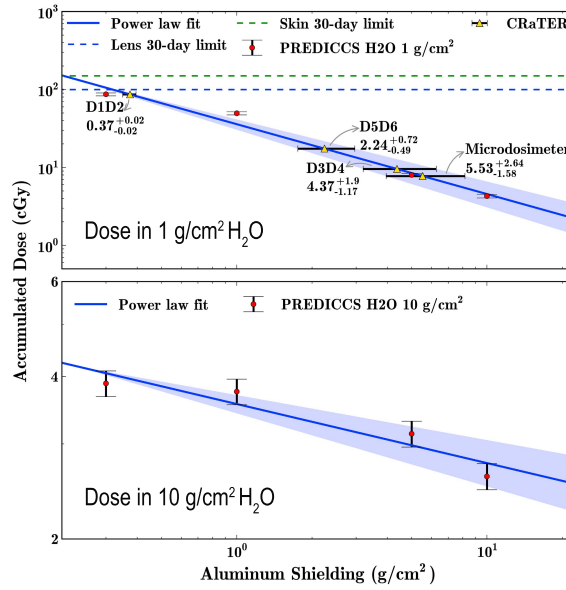


Figure 5. Accumulated doses on the lunar surface during the September 2017 SEP event behind different amounts of Al shielding. Red data points show PREDICCS data including uncertainties. The blue line and shaded uncertainty region shows power-law fit to the PREDICCS data, $D = D_0(s/s_0)^\gamma$, where D is dose, s is Al shielding thickness, and $s_0 = 1 \text{ g/cm}^2$. The fits have the following coefficients: (top) $D_0 = 35.91 \pm 5.45 \text{ cGy}$, $\gamma = -0.90 \pm 0.10$, (bottom) $D_0 = 3.56 \pm 0.14 \text{ cGy}$, $\gamma = -0.11 \pm 0.03$. In the top panel, we find the accumulated doses for D1—D2, D3—D4, and D5—D6 and the intersection with the power-law fit to estimate the effective shielding for each of these CRaTER thin-thick detector pairs. The numbers and uncertainties next to thin-thick detector pairs indicate effective Al shielding depth (in g/cm^2). In the bottom panel, we show PREDICCS data and the power-law fit for doses in $10 \text{ g/cm}^2 \text{ H}_2\text{O}$. Note that CRaTER detector pair dose rates are comparable to doses in the Lens and Skin ($\sim 1 \text{ g/cm}^2$ of H_2O as a proxy). However, the TEP between D1—D2 and D3—D4 is $\sim 6.09 \text{ g/cm}^2$ and therefore not sufficiently thick to evaluate the large internal mass ($\sim 10 \text{ g/cm}^2$ of H_2O as a proxy) associated with Organ and BFO doses. Therefore, the lower panel includes only PREDICCS data and the power-law fit, but does not contain CRaTER data.

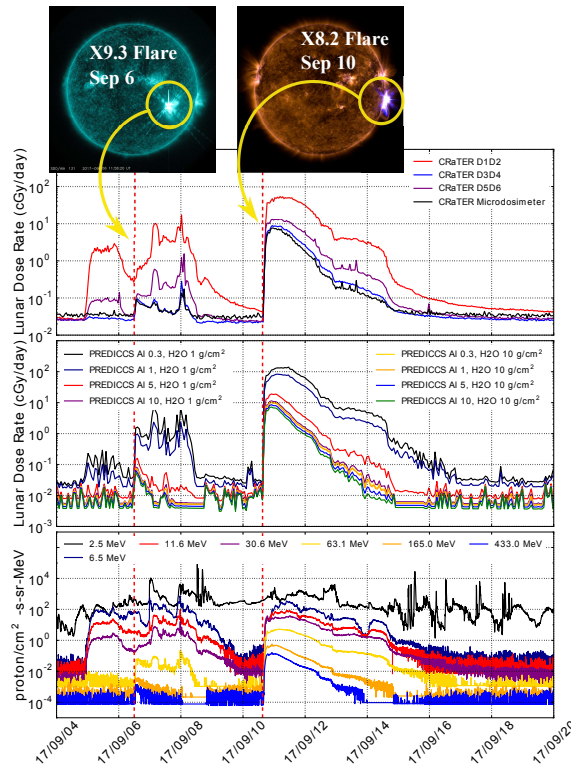


Figure 6. Large X-class flares began each of the major events observed in September 2017. The top panels include observations of the erupting active region observed by the Solar Dynamics Observatory (SDO), courtesy of NASA/SDO and the AIA, EVE, and HMI science teams. The left top solar image of the September 6 X9.3 flare (11:58 UT) is from telescope AIA 131. The top right image of the September 10 X8.2 flare (16:06) is a combination of wavelengths that includes AIA 193. Dose rates on the lunar surface from CRaTER (panel 2) and PREDICCS are shown throughout both events. Note that dose rates in free space are approximately $2\times$ those on the lunar surface. In the bottom panel, we show energetic particle differential fluxes from GOES.

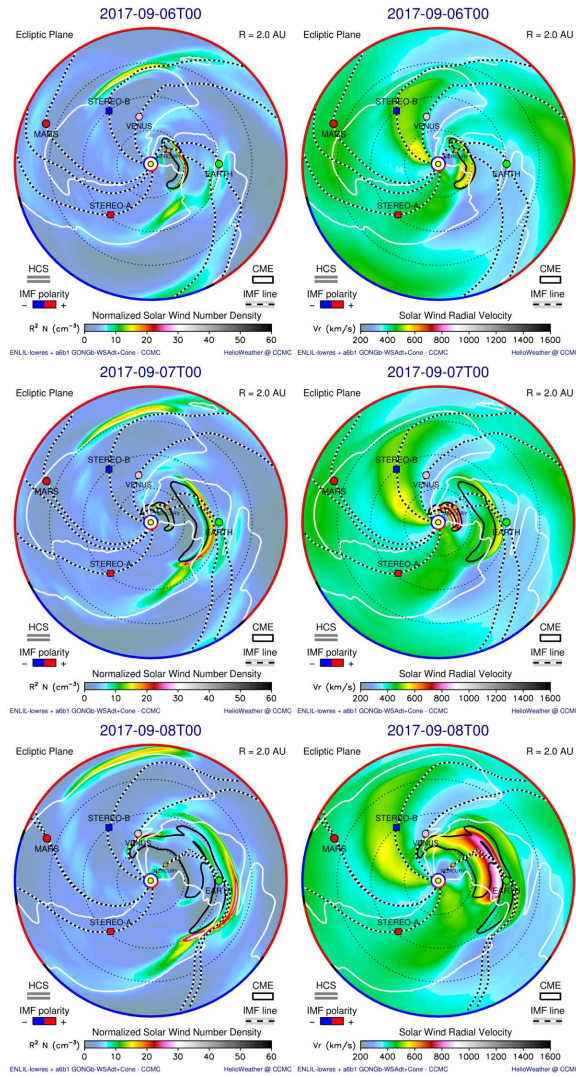


Figure 7. Propagation ICMEs from September 6 through September 8, 2017 based on WSA-ENLIL simulations. These CMEs followed the X9.3 flare event on September 6. The ICMEs over this period propagate toward Earth, and a strong compression region swept past Earth on September 7. These runs were performed by the CCMC.

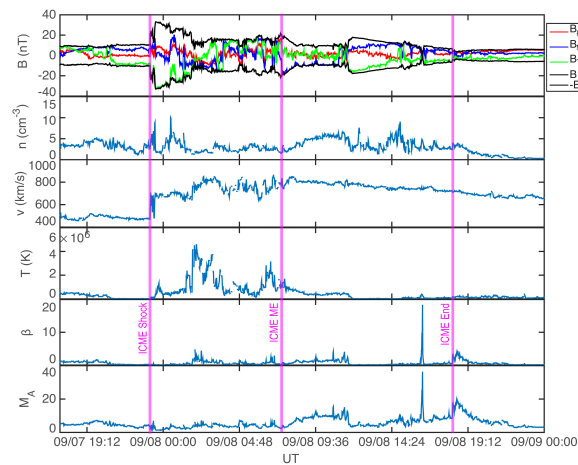


Figure 8. *In situ* plasma signatures of the ICME and Magnetic Ejecta (ME) observed on September 7 and 8. Pink vertical lines indicate the ICME start time, the ICME ME start time, and the ICME end time. The panels (top to bottom) correspond to: the solar wind magnetic field strength and RTN components, density, speed, temperature, plasma beta, and Alfvén mach number.

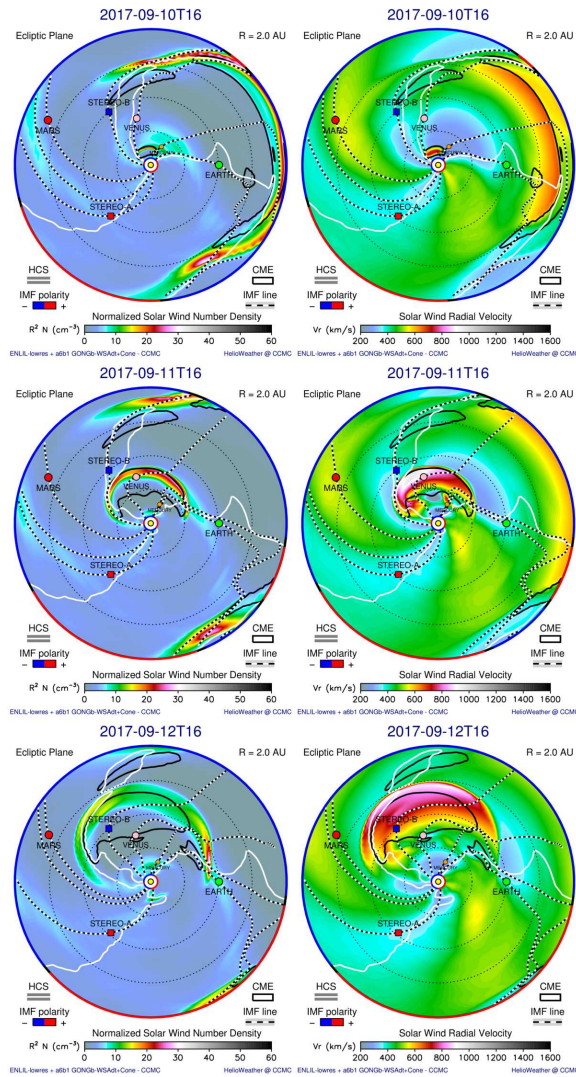


Figure 9. Propagation of ICMEs from September 10 (16:00 UT) through September 12 (16:00 UT), 2017 based on WSA-ENLIL simulations. These ICMEs followed the X8.2 flare event on September 10. The ICMEs over this period propagate toward the STEREO-B direction, at longitudes more than 90° larger than that of Earth. These runs were performed by the CCMC.

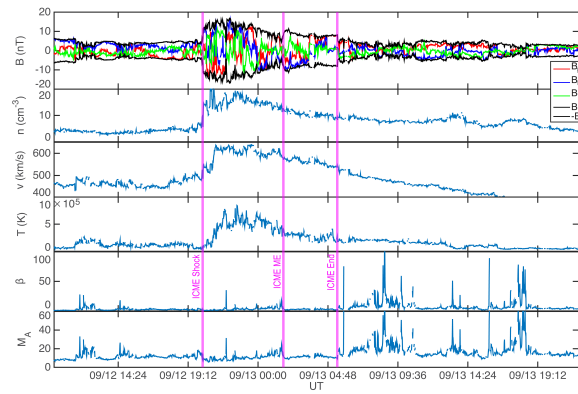


Figure 10. *In situ* plasma signatures of the ICME and Magnetic Ejecta (ME) observed on September 12 and 13. Pink vertical lines indicate the ICME start time, the ICME ME start time, and the ICME end time. The panels (top to bottom) correspond to: the solar wind magnetic field strength and RTN components, density, speed, temperature, plasma beta, and Alfvén mach number.

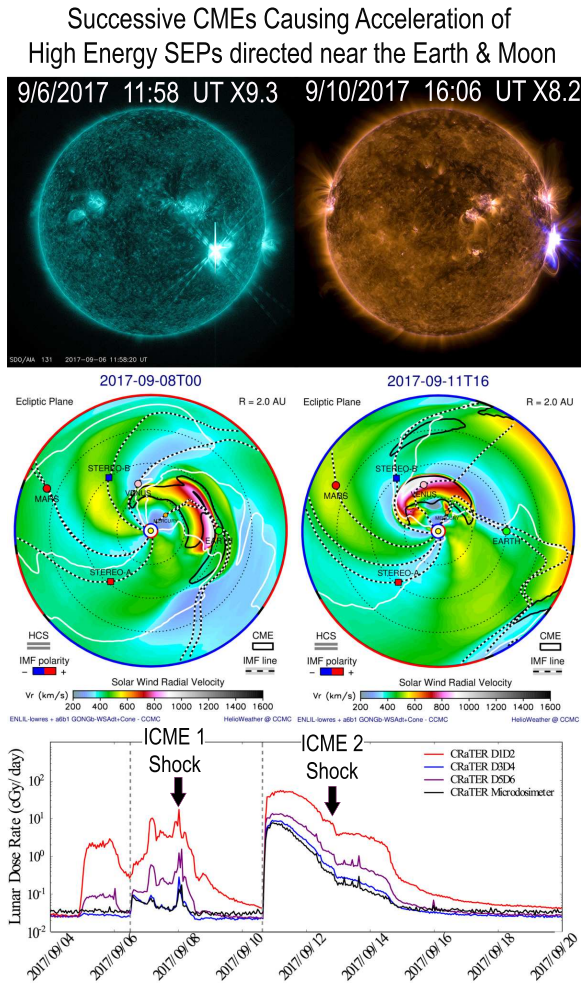


Figure 11. Summary of observations of the September 6 and September 10 SEP events. We note that the September 6 event resulted in a CME directed toward Earth, whereas the September 10 CME was directed 90° longitudinally forward. As a result, the first Earth directed event showed the passage of the CME, the associated shock and the energetic storm particles (ESP) accelerated in interplanetary space. In contrast, the September 10 SEP event did not show a pronounced shock-associated ESP enhancement in energetic particles.